Front. Phys., 2013, 8(3): 270–284
DOI 10.1007/s11467-013-0293-0

REVIEW ARTICLE

Higgs boson searches at the Tevatron

Gavin J. Davies†, on behalf of the CDF and D0 Collaborations

Imperial College London, London SW7 2AZ, United Kingdom

E-mail: †g.j.davies@imperial.ac.uk

Received December 18, 2012; accepted January 6, 2013

This article reviews the Higgs searches at the Tevatron, as presented over the summer of 2012; both standard model (SM) and beyond the standard model (BSM) results are discussed as detailed (arXiv: 1207.0449; Phys. Rev. Lett., 2012, 109: 071804; Phys. Rev. D, 2012, 85: 032005). We discuss the combination of searches by the CDF and D0 Collaborations for the standard model Higgs boson in the mass range 100–200 GeV/c^2 produced in the the $gg \to H$, WH, ZH, $t\bar{t}H$, and vector boson fusion production modes, and decaying in the $H \to b\bar{b}$, $H \to W^+W^-$, $H \to ZZ$, $H \to \tau^+\tau^-$, and $H \to \gamma\gamma$ modes. The data, collected at the Fermilab Tevatron collider in $p\bar{p}$ collisions at $\sqrt{s} = 1.96$ TeV, correspond to integrated luminosities of up to 10 fb^{-1}. In the absence of signal, we expect to exclude the regions $100 < m_H < 120$ GeV/c^2 and $139 < m_H < 184$ GeV/c^2. We exclude, at the 95% C.L., two regions: $100 < m_H < 103$ GeV/c^2, and $147 < m_H < 180$ GeV/c^2. We observe a significant excess of events in the mass range between 115 and 140 GeV/c^2. The local significance corresponds to 3.0 standard deviations at $m_H = 120$ GeV/c^2; the global significance (incorporating the look-elsewhere effect) for such an excess anywhere in the full mass range investigated is approximately 2.5 standard deviations. Furthermore, we separately combine searches for $H \to b\bar{b}$, $H \to W^+W^-$ and $H \to \gamma\gamma$. We find that the excess is concentrated in the $H \to b\bar{b}$ channel, appearing in the searches over a broad range of m_H; the maximum local significance of 3.3 standard deviations corresponds to a global significance of approximately 3.1 standard deviations. The observed signal strengths in all channels are consistent with the expectation for a standard model Higgs boson at $m_H = 125$ GeV/c^2. The production of neutral Higgs bosons in association with b-quarks can be significantly enhanced in various beyond the standard model scenarios, including Supersymmetry. The recent combination of such searches from the two collaborations is discussed.

Keywords Higgs, Tevatron

PACS numbers 13.85.Rm, 14.80.Bn, 12.38.Qk, 12.60.Fr

Contents

1 Introduction

Within the standard model (SM) [4–6], spontaneous breaking of electroweak symmetry gives mass to the W and Z bosons [7–10], and to the fundamental fermions. In the SM, the symmetry-breaking mechanism predicts the existence of a neutral scalar particle, the Higgs boson,

and its mass (m_H) is a free parameter.

Precision electroweak data, including the recently updated measurements of the W-boson and top quark masses from the CDF and D0 Collaborations [11, 12], yield an indirect constraint on the allowed mass of the Higgs boson, $m_H < 152$ GeV/c^2 [13], at the 95% confidence level (C.L.). Direct searches at LEP2 exclude SM Higgs boson masses below 114.4 GeV/c^2 [14]. The ATLAS and CMS Collaborations have recently reported the observation of a new boson with mass of around 125 GeV/c^2 [15, 16] at the Large Hadron Collider (LHC). Much of the sensitivity of the LHC searches comes from gluon-gluon fusion ($gg \to H$) production and Higgs boson decays to $\gamma\gamma$, ZZ, and W^+W^- boson pairs, which probe the couplings of the Higgs boson to other bosons. Within the context of the SM, the $gg \to H$ production mechanism is dominated by processes with one quark loop, and is therefore sensitive almost exclusively to the couplings of the Higgs boson to fermions. Direct searches for associated production $VH \to Vb\bar{b}$ at the LHC, where $V = W$ or Z [17, 18], are not yet sensitive to SM Higgs boson production. The CDF and D0 Collaborations have recently reported combined evidence for a particle, with a mass consistent with that of the new boson observed at LHC, produced in association with weak bosons and decaying to a bottom–antibottom quark pair [2].

In this article, we discuss the results of SM Higgs boson searches in $p\bar{p}$ collisions at $\sqrt{s} = 1.96$ TeV using Tevatron Run II integrated luminosities of up to 10 fb^{-1} per experiment, as presented over the summer of 2012, and documented in Ref. [1]. The analyses combined seek signals of Higgs bosons in the mass range 100–200 GeV/c^2, produced in association with a vector boson ($q\bar{q} \to VH$), in association with top quarks, through gluon-gluon fusion, and through vector boson fusion (VBF) ($q\bar{q} \to q'\bar{q}'H$). The Higgs boson decay modes studied are $H \to b\bar{b}$, $H \to W^+W^-$, $H \to ZZ$ and $H \to \gamma\gamma$. When results are shown for the $H \to b\bar{b}$ mode alone, these are taken from Ref. [2] (as shown at SUSY12), and so differ slightly from those in Ref. [1]. For Higgs boson masses greater than 125 GeV/c^2, searches for $H \to W^+W^-$ decays followed by leptonic W decays provide the greatest sensitivity. Below 125 GeV/c^2 sensitivity comes mainly from associated production VH with the H boson decaying to $b\bar{b}$ and the W or Z boson decaying leptonically. Both collaborations consider the processes $WH \to \ell\nu b\bar{b}$, $ZH \to \ell^+\ell^- b\bar{b}$, and $WH, ZH \to \not\!\!E_T b\bar{b}$ (where ℓ is either e or μ and $\not\!\!E_T$ denotes missing transverse energy [19]).

2 Event simulation

Higgs boson signal events are simulated using the leading order (LO) calculation from PYTHIA [20], with CTEQ5L (CDF) and CTEQ6L1 (D0) [21, 22] parton distribution functions (PDFs). The normalization of these Monte Carlo (MC) samples is obtained using the highest-order cross section calculation available for the corresponding production process. The cross section for the gluon-gluon fusion process is calculated at next-to-next-to-leading order (NNLO) in quantum chromodynamics (QCD) with soft gluon resummation to next-to-next-to-leading-log (NNLL) accuracy [23, 24]. The WH and ZH cross section calculations are performed at NNLO precision in QCD and next-to-leading-order (NLO) precision in the electroweak corrections [25, 26]. The VBF cross section is computed at NNLO in QCD [27], and the electroweak corrections computed with the HAWK program [28, 29]. All signal production cross sections are computed using the MSTW2008 PDF set [30]. The PDF uncertainties are assessed following Refs. [31–33]. The Higgs boson branching fractions are from Ref. [34] and rely on calculations using HDECAY [35] and PROPHECY4F [36, 37]. The distribution of the transverse momentum (p_T) of the Higgs boson in the PYTHIA-generated gluon-gluon fusion sample is reweighted to match the p_T as calculated by HQT, at NNLL and NNLO accuracy [38, 39].

We model SM and instrumental background processes using a mixture of MC and data-driven methods. For CDF, backgrounds from SM processes with electroweak gauge bosons or top quarks are modeled using PYTHIA, ALPGEN [40], MC@NLO [41], and HERWIG [42]. For D0, these backgrounds are modeled using PYTHIA, ALPGEN, and SINGLETOP [43–45]. An interface to PYTHIA provides parton showering and hadronization for generators without this functionality.

The effects of instrumental noise and additional $p\bar{p}$ interactions are modeled using MC in CDF while in D0 recorded data from randomly selected beam crossings with the same luminosity profile as data are added to the MC events.

Diboson (WW, WZ, ZZ) MC samples are normalized using the NLO calculations from MCFM [46]. For top quark pair production ($t\bar{t}$), we use a production cross section of 7.04 ± 0.70 pb [47], which is based on a top-quark mass of 173 GeV/c^2 [12] and MSTW 2008 PDFs [30]. The single-top-quark production cross section is taken to be 3.15 ± 0.31 pb [48]. For many analyses, the V+jet processes are normalized using the NNLO cross section calculations of Ref. [49], though in some cases data-driven techniques are used. Likewise, the normalization of the instrumental, multijet and, at CDF, the V+heavy-flavor jet backgrounds [50] are constrained from data samples where the expected signal to background ratio is several orders of magnitude smaller than in the search samples. At D0, the V+heavy-flavor normalization, relative

to V+light-flavor, is taken from MCFM. In addition, at D0, prior to b-tagging [51] V+jets samples are compared to data and corrections applied to mitigate any discrepancies in kinematic distributions.

For the $H \to W^+W^-$ analyses the dominant irreducible background process is diboson production, while the dominant reducible backgrounds are Z/γ^*+jets, W+jets, $t\bar{t}$, and multijet production where jets can be misidentified as leptons. For the analyses targeting $H \to b\bar{b}$ the main backgrounds originate from V+heavy-flavor-jets and $t\bar{t}$ production.

3 Event selection

The CDF and D0 detectors are multipurpose spectrometers surrounded by hermetic calorimeters and muon detectors and are designed to study the products of 1.96 TeV proton-antiproton collisions [52–56]. Event selections are similar in the CDF and D0 analyses, typically consisting of a preselection based on event topology and kinematics, and a final subsequent selection using multivariate analysis (MVA) techniques [57] that combine several discriminating variables into a single final discriminant to separate signal from background. Each channel is divided into exclusive sub-channels according to various lepton, jet multiplicity, and b-tagging characterization criteria. This procedure groups events with similar signal-to-background ratio to optimize the overall sensitivity. Such subdivision allows, for example, the efficient use of poorly reconstructed leptons or those in the forward region, the exploitation of the different dominant signal and backgrounds when training the MVAs separately in each sub-channel, or reduction of the impact of systematic uncertainties. The MVAs are trained separately at each value of m_H in their respective mass ranges, in 5 GeV/c^2 steps.

For the analyses exploiting the $H \to b\bar{b}$ decay, b-tagging and mass resolution are of great importance. Both collaborations have developed multivariate approaches to maximize the performance of the b-tagging algorithms. In the D0 analyses, the MVA builds and improves upon the previous neural network b-tagger [58] and achieves an identification efficiency of about 80% for b-jets with a misidentification rate for light (u, d, s, and gluon) jets of about 10%. The CDF b-tagging algorithm has been augmented with an MVA [59–61], providing a b-tagging efficiency of about 70% and a misidentification rate for light jets of about 5%. (The $WH, ZH \to \not\!\!E_T b\bar{b}$ channel does not use the updated b-tagger for the results discussed here). The decay width of the SM Higgs boson is predicted to be much smaller than the experimental dijet mass resolution, which is typically 15% of the mean reconstructed mass. A SM Higgs boson signal would appear as a broad enhancement in the reconstructed di-b-jet mass distribution. CDF and D0 search for $H \to b\bar{b}$ produced in association with a leptonically decaying $W^{\pm}$ boson or a leptonically or invisibly decaying Z boson. CDF also contributes a search for $t\bar{t}H \to t\bar{t}b\bar{b}$, in which one of the top quarks decays to a leptonically-decaying W boson.

Both collaborations target the $H \to W^+W^-$ signal in which both W bosons decay leptonically by selecting events with large missing transverse energy and two oppositely charged, isolated leptons. The presence of neutrinos in the final state prevents full reconstruction of the Higgs boson mass. Other observables are used for separating the signal from background. For example, the azimuthal angle between the leptons in signal events is smaller on average than that in background events due to the scalar nature of the Higgs boson and parity violation in $W^{\pm}$ decays. Furthermore, the missing transverse momentum is larger, and the total transverse energy of the jets is lower, than they are typically in background events.

Although the primary sensitivity at low mass ($m_H \leqslant 125$ GeV/c^2) is provided by the $H \to b\bar{b}$ analyses and at high mass ($m_H > 125$ GeV/c^2) by the $H \to W^+W^-$ analyses, significant additional sensitivity is achieved by the inclusion of other channels. Both collaborations contribute analyses searching for Higgs bosons decaying into diphoton pairs, tau pairs and tri-lepton searches. The full list of channels included in the combination over the full mass range from 100–200 GeV/c^2 can be found in Ref. [1]. The $H \to b\bar{b}$ specific results use slightly updated inputs, as detailed in Ref. [2], with further details in Refs. [63, 64] and references therein.

4 Statistical techniques

The results are interpreted using both Bayesian and modified frequentist techniques, separately at each value of m_H, as was done previously e.g. [2]. The two methods yield results that are numerically consistent; limits on the Higgs boson production rate typically agree within 10% at each value of m_H, and within 1% on average. For simplicity, when summarizing the results, we quote one set of values as the default, and the *a priori* decision made for the earlier Tevatron combinations to use the Bayesian method is retained here. Both methods use the distributions of the final discriminants, and not only the total event counts passing selection requirements.

Each of the techniques is built on a combined likelihood [including priors on systematic uncertainties, $\pi(\vec{\theta})$] based on the product of likelihoods for the individual

channels, each of which is a product over histogram bins:

$$\mathcal{L}(R,\vec{s},\vec{b}|\vec{n},\vec{\theta})\times\pi(\vec{\theta})=\prod_{i=1}^{N_{\rm C}}\prod_{j=1}^{N_{\rm bins}}\mu_{ij}^{n_{ij}}\frac{{\rm e}^{-\mu_{ij}}}{n_{ij}!}\times\prod_{k=1}^{n_{\rm sys}}{\rm e}^{-\theta_k^2/2} \quad (1)$$

where the first product is over the number of channels ($N_{\rm C}$), and the second product is over histogram bins containing n_{ij} events, binned in ranges of the final discriminants used for the individual analyses. The predictions for the bin contents are $\mu_{ij}=R\times s_{ij}(\vec{\theta})+b_{ij}(\vec{\theta})$ for channel i and histogram bin j, where s_{ij} and b_{ij} represent the expected SM signal and background in the bin, and R is a scaling factor applied to the signal. By scaling all signal contributions by the same factor we make the assumption that the relative contributions of the different processes at each m_H are as given by the SM. Systematic uncertainties are parameterized by the dependence of s_{ij} and b_{ij} on $\vec{\theta}$. Each of the $n_{\rm sys}$ components of $\vec{\theta}$, θ_k, corresponds to a single independent source of systematic uncertainty scaled by its standard deviation, and each parameter may affect the predictions of several sources of signal and background in different channels, thus accounting for correlations. Gaussian priors are assumed for the nuisance parameters, truncated to ensure that no prediction is negative.

In the Bayesian technique, we assume a uniform prior for non-negative values of R and integrate the likelihood function multiplied by the priors for the nuisance parameters to obtain the posterior density for R. The observed 95% credibility level upper limit on R, $R_{95}^{\rm obs}$, is such that 95% of the integral of the posterior of R is below $R_{95}^{\rm obs}$. The expected distribution of R_{95} is computed in an ensemble of simulated experimental outcomes assuming no signal is present. In each simulated outcome, random values of the nuisance parameters are drawn from their priors. A combined measurement of the cross section for Higgs boson production times the branching fraction $\mathcal{B}(H\to XX)$, in units of the SM production rate, is given by $R^{\rm fit}$, which is the value of R that maximizes the posterior density. The 68% credibility interval, which corresponds to one standard deviation (s.d.), is quoted as the smallest interval containing 68% of the integral of the posterior.

We also perform calculations using the modified frequentist technique [62], CL$_{\rm s}$, using a log-likelihood ratio (LLR) as the test statistic: LLR$=-2\ln\frac{p({\rm data}|s+b)}{p({\rm data}|b)}$, where $p({\rm data}|s+b)$ and $p({\rm data}|b)$ are the probabilities that the data (either simulated pseudodata or the actual observed data) are drawn from distributions predicted under the signal-plus-background and background-only hypotheses respectively. The probabilities p are computed using the best-fit values of the parameters θ_k, separately for each of the two hypotheses [65]. The use of these fits extends the procedure used at LEP [66, 67], improving the sensitivity when the expected signals are small and the uncertainties on the backgrounds are large. The CL$_s$ technique involves computing two p-values, CL$_b=p$ (LLR$\geqslant$ LLR$_{\rm obs}|b$), where LLR$_{\rm obs}$ is the value of the test statistic computed for the data, and CL$_{s+b}=p$ (LLR$\geqslant$ LLR$_{\rm obs}|s+b$). To compute limits, we use the ratio of p-values, CL$_s=$ CL$_{s+b}$/CL$_b$. If CL$_s<0.05$ for a particular choice of the signal-plus-background hypothesis, parameterized by the signal scale factor R, that hypothesis is excluded at least at the 95% C.L. The value of $R_{95}^{\rm obs}$ in the CL$_{\rm s}$ method is the smallest value of R excluded at the 95% C.L. The expected limit is computed using the median LLR value expected in the background-only hypothesis. Systematic uncertainties are included by fluctuating the predictions for s_{ij} and b_{ij} when generating the pseudoexperiments used to compute CL$_{s+b}$ and CL$_b$.

5 Systematic uncertainties

Systematic uncertainties are evaluated for each final state, background, and signal process. Uncertainties that modify only the normalization and uncertainties that change the shape of the final discriminant distribution are included. In order to study the "shape" uncertainties on the distributions of the final discriminants, the relevant parameter is varied within one standard deviation of its uncertainty and the full analysis repeated using the modified kinematics. For example, for the jet energy scale and jet energy resolution, the parameters of the energy scale and resolution are varied within 1 s.d. of their uncertainties and the analysis carried out using the kinematics of the modified jets, also including the effects of events which enter or leave the selected samples as the jet energy parameters are changed. No retraining of the MVAs is performed during the propagation of systematic uncertainties to the distributions of the discriminants. Correlations between signal and background, across different channels within an experiment and across the two experiments are taken into account.

The uncertainties on the inclusive signal production cross sections are estimated from the variations in the factorization and renormalization scale, which include the impact of uncalculated higher-order corrections, uncertainties due to PDFs, and the dependence on the strong coupling constant, α_s, as recommended by the PDF4LHC working group [31, 32]. The resulting uncertainties on the inclusive VH and VBF production rates are taken to be 7% and 5%, respectively [25, 26].

For analyses seeking $gg\to H$ production that divide events into categories based on the number of reconstructed jets, the uncertainties associated with the renormalization and factorization scale are estimated follow-

ing Ref. [68]. By propagating the uncorrelated uncertainties of the NNLL inclusive [23, 24], NLO $\geqslant 1$ jet [33], and NLO $\geqslant 2$ jets [69] cross sections to the exclusive $gg \to H + 0$ jet, 1 jet, and $\geqslant 2$ jets rates, an uncertainty matrix containing correlated and uncorrelated uncertainty contributions between exclusive jet categories is obtained. The PDF uncertainties are evaluated following Refs. [23, 33].

Significant sources of uncertainty for all analyses are the integrated luminosities, used to normalize the expected signal yield and MC-based backgrounds, and the cross-sections for the simulated backgrounds. For the former, uncertainties of 6% (CDF) and 6.1% (D0) are used, with 4% arising from the inelastic $p\bar{p}$ cross section which is taken to be 100% correlated between CDF and D0. Cross section uncertainties of 6% and 7% are used for diboson and $t\bar{t}$ production respectively.

Sources of systematic uncertainty that affect both the normalization and the shape of the final discriminant distribution include jet energy scale 1%–4%, jet energy resolution 1%–3%, lepton identification, trigger efficiencies, and b-tagging. Uncertainties on lepton identification and trigger efficiencies range from 2% to 6% and are applied to both the signal and MC-based background predictions. These uncertainties are estimated from data-based methods separately by CDF and D0, and differ based on lepton flavor and identification category. The b-tag efficiencies and mistag rates are similarly constrained by auxiliary data samples, such as inclusive jet data or $t\bar{t}$ events. The uncertainty on the per-jet b-tag efficiency is approximately 4%, and the mistag uncertainties vary between 7% and 15%.

For the analyses targeting the $H \to b\bar{b}$ decay, the largest sources of uncertainty on the dominant backgrounds are the rates of tagged V+heavy-flavor jets, which are typically 20%–30% of the predicted values. Following constraint by the data, the uncertainties on these rates are typically 8% or less. The data samples in the V+jets selections prior to b-tagging are used as control samples to constrain systematic uncertainties in the Monte Carlo modeling of the energies and angles of jets. Any residual discrepancy coming from the difference between light- and heavy-flavor components has been shown to be smaller than the systematic uncertainties associated with the generator or the correction procedures themselves.

6 Results – Standard model interpretation

6.1 Diboson production

To validate the background modeling and methodology described in this article, independent measurements of SM diboson production in the same final states used for the SM Higgs searches are carried out. The high mass analyses measure the $p\bar{p} \to W^+W^-$ cross section, whilst the low mass analyses target VZ production in the $Z \to b\bar{b}$ final state. The data sample, reconstruction, process modeling, uncertainties, and sub-channel divisions are identical to those of the SM Higgs boson searches. However, discriminant functions are trained to distinguish the contributions of SM diboson production from those of other backgrounds, and potential contributions from Higgs boson production are not considered. By way of illustration, below, we focus on VZ production.

The NLO SM cross section for VZ production times the branching fraction of $Z \to b\bar{b}$ is 0.68 ± 0.05 pb. This is about six times larger than the 0.12 ± 0.01 pb cross section times branching fraction of $VH(H \to b\bar{b})$ for a 125 GeV/c^2 SM Higgs boson, but the associated background is about four times larger. WW production is considered as background. The measured cross section for VZ is 3.9 ± 0.6 (stat) ± 0.7 (syst) pb, which is consistent with the SM prediction of 4.4 ± 0.3 pb. The combined background-subtracted reconstructed dijet mass distribution for the VZ analysis is shown in Fig. 1. The VZ signal and the background contributions are fit to the data, and the fitted background is then subtracted. Also shown is the contribution expected from a SM Higgs boson with $m_H = 120$ GeV/c^2.

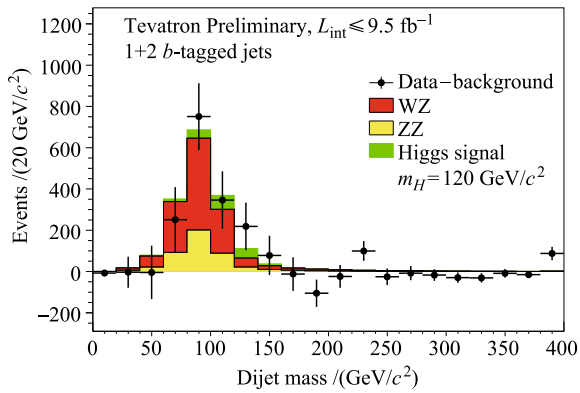

Fig. 1 Background-subtracted distribution of the reconstructed dijet mass, summed over all input channels. The VZ signal and the background contributions are fit to the data, and the fitted background is subtracted. The fitted VZ and expected SM Higgs ($m_H = 120$ GeV/c^2) contributions are shown with filled histograms. Reproduced from Ref. [1].

6.2 Full combination

The results produced by the multivariate Higgs analyses can be visualized by combining the histograms of the final discriminants, adding the contents of bins with similar signal-to-background ratio (s/b). Classification in this way preserves the importance of each of the events in the

histogram, to the extent that they are not added to other events that are selected with different s/b. The resulting distribution of $\log_{10}(s/b)$ is shown for $m_H = 125$ and 165 GeV/c^2 in Fig. 2, demonstrating agreement with background over five orders of magnitude. In the highest s/b bins an excess of events above the background expectation is seen for the analyses seeking a Higgs boson with mass of 125 GeV/c^2.

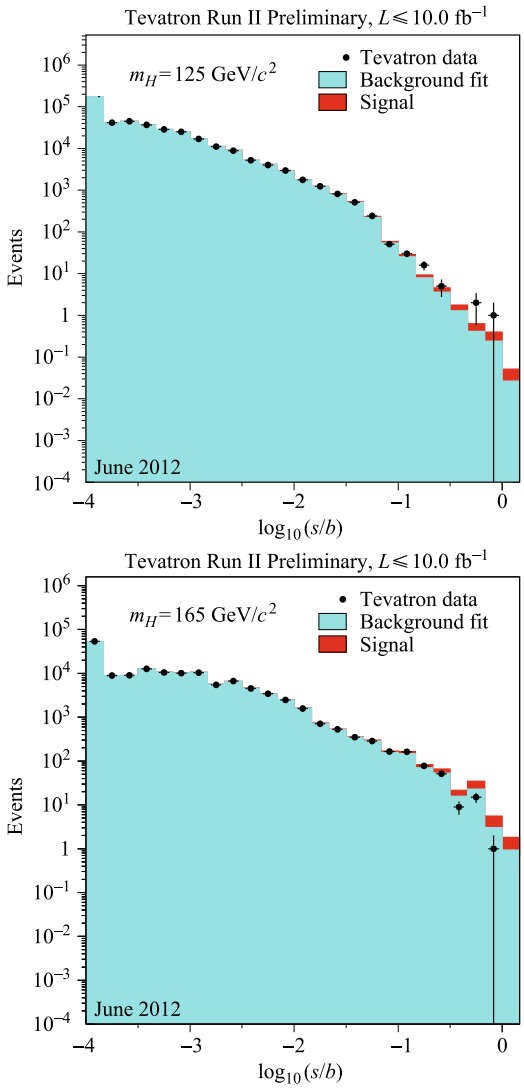

Fig. 2 Distributions of $\log_{10}(s/b)$, for the data from all contributing channels from CDF and D0, for Higgs boson masses of 125 and 165 GeV/c^2. The data are shown with points, and the expected signal is shown stacked on top of the backgrounds, which have been fit to the data within their systematic uncertainties. Underflows and overflows are collected into the leftmost and rightmost bins, respectively. Reproduced from Ref. [1].

Figure 3 shows the signal expectation and the data with the background subtracted, as a function of the s/b of the collected bins, for the combined search for a Higgs boson with mass $m_H = 125$ and 165 GeV/c^2. The background model is fit to the data, floating the nuisance parameters within their constraints, and the uncertainties on the background predictions in each bin are those after the fit. An excess of events in the highest s/b bins relative to the background-only expectation is observed for the analyses seeking a Higgs boson of mass 125 GeV/c^2, whilst a deficit is seen for the analyses seeking a Higgs boson of mass 165 GeV/c^2.

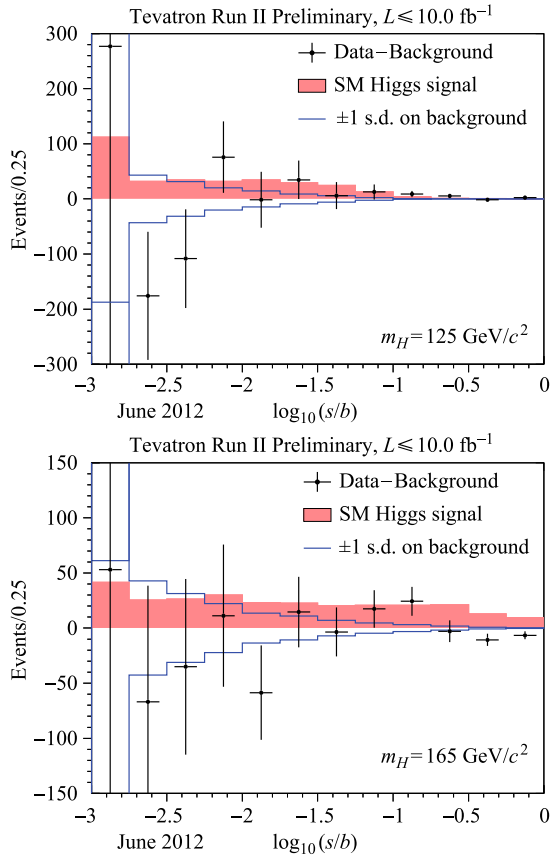

Fig. 3 Background-subtracted data distributions for all channels, summed in bins of s/b, for Higgs boson masses of 125 and 165 GeV/c^2. The background has been fit, within its systematic uncertainties and assuming no Higgs boson signal is present, to the data. The points with error bars indicate the background-subtracted data; the sizes of the error bars are the square roots of the predicted background in each bin. The unshaded (*blue-outline*) histogram shows the systematic uncertainty on the best-fit background model, and the shaded histogram shows the expected signal for a standard model Higgs boson. Reproduced from Ref. [1].

Figure 4 displays the LLR distributions for the combined analyses as a function of m_H. Included are the median of the LLR distributions for the background-only hypothesis (LLR_b), the signal-plus-background hypothesis (LLR_{s+b}), and the observed value for the data ($\mathrm{LLR}_{\mathrm{obs}}$). The shaded bands represent the one and two s.d. departures for LLR_b centered on the median. These results are also listed in Table 1. The separation between the medians of the LLR_b and LLR_{s+b} distributions provides a measure of the discriminating power of the search. The sizes of the one- and two-s.d. LLR_b bands indicate

the width of the LLR_b distribution, assuming no signal and only statistical fluctuations and systematic effects are present. The value of $\mathrm{LLR}_{\mathrm{obs}}$ relative to LLR_{s+b} and LLR_b indicates whether the data distribution more closely resembles what we expect if a signal is present (i.e., the LLR_{s+b} distribution, which is negative by construction) or the background-only expectation. The significance of departures of $\mathrm{LLR}_{\mathrm{obs}}$ from LLR_b can be evaluated by the width of the LLR_b bands. The separation of the signal-plus-background and background-only hypotheses is greater than two s.d. up to ~ 185 GeV/c^2. The data are consistent with the background-only hypothesis (the black dashed line) below ~ 115 GeV/c^2 and above approximately 145 GeV/c^2. A slight excess is seen above approximately 195 GeV/c^2, where our ability to separate the two hypotheses is limited. For m_H from 115 to 140 GeV/c^2, a significant excess in the data above the SM background is observed.

Motivated by the excess in the data in the low-m_H region of our searches, we compare the observed LLR with that expected if an SM Higgs boson was present with a mass of $m_H = 125$ GeV/c^2. Figure 5 shows the same

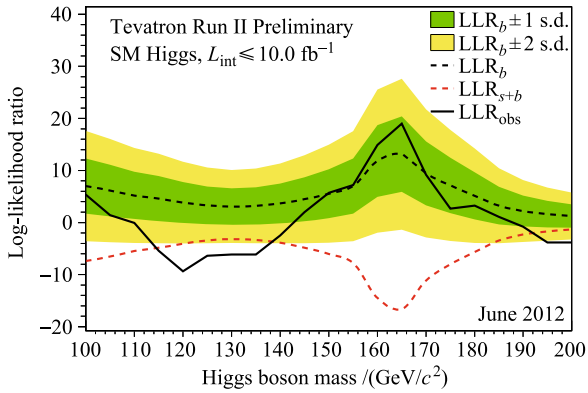

Fig. 4 The log-likelihood ratio LLR as a function of Higgs boson mass. The solid line shows the observed LLR values, the dark dashed line shows the median expectation assuming no Higgs boson signal is present, and the dark and light-shaded bands correspond to the regions encompassing one and two s.d. fluctuations around the background expectation. The red short-dashed line shows the median expectation assuming a Higgs boson signal is present at each value of m_H in turn. Reproduced from Ref. [1].

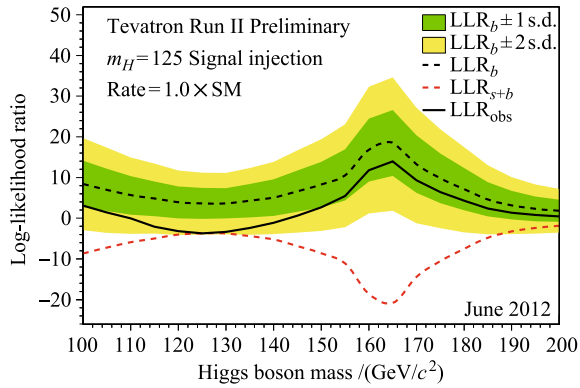

Fig. 5 The log-likelihood ratio (LLR) distributions as in Fig. 4. The thick black curve shows the median expected outcome assuming a Higgs boson of mass $m_H = 125$ GeV/c^2 is present. The green and yellow bands correspond to the regions enclosing 1 s.d. and 2 s.d. fluctuations around the median expected value assuming only background is present, respectively. The red dashed curve shows the median expected value assuming a Higgs boson signal is present, separately at each m_H. Reproduced from Ref. [1].

Table 1 Log-likelihood ratio (LLR) values for the combined CDF and D0 Higgs boson search obtained using the CL_S method.

m_H/(GeV/c^2)	$\mathrm{LLR}_{\mathrm{obs}}$	LLR_{s+b}	$\mathrm{LLR}_b^{-2\sigma}$	$\mathrm{LLR}_b^{-1\sigma}$	LLR_b	$\mathrm{LLR}_b^{+1\sigma}$	$\mathrm{LLR}_b^{+2\sigma}$
100	5.36	−7.41	17.61	12.31	7.02	1.72	−3.58
105	1.44	−6.53	16.08	11.12	6.16	1.19	−3.77
110	−0.05	−5.49	14.32	9.76	5.20	0.64	−3.92
115	−5.41	−4.86	13.21	8.91	4.62	0.32	−3.98
120	−9.39	−4.06	11.68	7.76	3.84	−0.08	−4.00
125	−6.39	−3.43	10.56	6.93	3.30	−0.33	−3.97
130	−6.12	−3.18	10.09	6.58	3.07	−0.43	−3.94
135	−6.12	−3.34	10.36	6.78	3.20	−0.38	−3.96
140	−2.46	−3.87	11.33	7.50	3.67	−0.16	−3.99
145	1.99	−4.83	12.95	8.71	4.48	0.25	−3.99
150	5.73	−6.05	14.94	10.24	5.53	0.83	−3.88
155	7.21	−7.78	17.57	12.28	6.99	1.70	−3.58
160	14.92	−14.47	25.57	18.69	11.82	4.94	−1.93
165	18.98	−16.61	27.63	20.38	13.13	5.88	−1.36
170	9.15	−11.13	21.74	15.59	9.44	3.30	−2.85
175	2.66	−8.04	17.81	12.47	7.13	1.79	−3.55
180	3.26	−5.68	14.21	9.68	5.14	0.61	−3.93
185	1.07	−3.46	10.45	6.85	3.24	−0.36	−3.96
190	−0.78	−2.31	8.15	5.18	2.21	−0.76	−3.74
195	−3.84	−1.69	6.72	4.17	1.63	−0.92	−3.47
200	−3.82	−1.31	5.76	3.51	1.26	−0.98	−3.23

median expectation curves as Fig. 4, but in the place of the data, the median expected LLR assuming a Higgs boson signal is present at $m_H = 125$ GeV/c^2 is shown. This signal-injected-LLR curve has a similar shape to the observed one. While the search for a 125 GeV/c^2 Higgs boson is optimized to find a Higgs boson of that mass, the excess of events over the SM background estimates also affects the results of Higgs boson searches at other masses. Nearby masses are the most affected, but the expected presence of $H \to W^+W^-$ decays for a 125 GeV/c^2 Higgs boson implies a small expected excess in the $H \to W^+W^-$ searches at all masses due to the poor reconstructed mass resolution in this final state.

The limit on SM Higgs boson production as a function of m_H is extracted in the range 100–200 GeV/c^2 in terms of $R_{95}^{\rm obs}$, the ratio of the observed limit to the predicted SM rate.

The expected and observed ratios to the SM cross section for the combined CDF and D0 analyses are shown in Fig. 6, and listed in Table 2 for both the Bayesian and the $\rm CL_s$ methods. We quote, in the summary below, only the limits obtained with the Bayesian method, which was decided upon *a priori*.

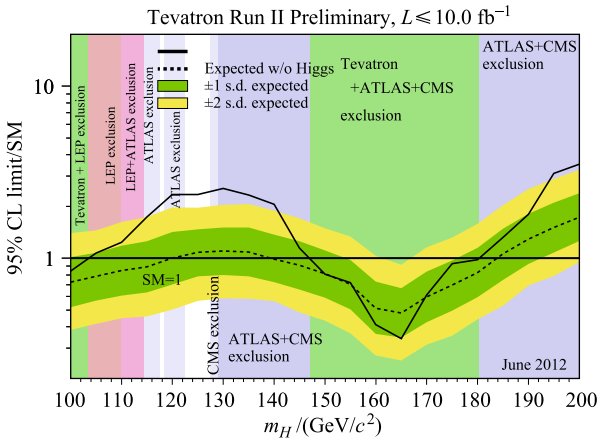

Fig. 6 Observed and expected (median, for the background-only hypothesis) 95% C.L. Bayesian upper limits expressed as a multiple of the SM cross section for test masses every 5 GeV/c^2. The points are joined by straight lines for better readability. The bands indicate the 1 and 2 s.d. probability regions where the limits can fluctuate, in the absence of signal. Reproduced from Ref. [1].

Intersections of piecewise linear interpolations of our observed and expected rate limits with the SM=1 line are used to quote ranges of Higgs boson masses that are excluded and that are expected to be excluded, extending the results from the 5 GeV/c^2 mass points investigated to the intervals in between. The regions of Higgs boson masses excluded at the 95% C.L. thus obtained are $100 < m_H < 103$ GeV/c^2 and $147 < m_H < 180$ GeV/c^2. The expected exclusion regions are $100 < m_H < 120$ GeV/c^2 and $139 < m_H < 184$ GeV/c^2.

Table 2 Ratios of median expected and observed 95% C.L. limit to the SM cross section for the combined CDF and D0 analyses as a function of the Higgs boson mass in GeV/c^2, obtained with the Bayesian and $\rm CL_s$ methods.

m_H/(GeV/c^2)	Bayesian		$\rm CL_s$	
	$R_{95}^{\rm obs}$	$R_{95}^{\rm exp}$	$R_{95}^{\rm obs}$	$R_{95}^{\rm exp}$
100	0.84	0.73	0.80	0.73
105	1.07	0.78	1.08	0.78
110	1.24	0.85	1.26	0.85
115	1.74	0.89	1.86	0.91
120	2.35	1.00	2.49	1.00
125	2.35	1.08	2.42	1.08
130	2.55	1.10	2.57	1.12
135	2.33	1.09	2.46	1.10
140	2.06	0.99	1.94	1.02
145	1.14	0.91	1.13	0.92
150	0.81	0.81	0.80	0.82
155	0.72	0.71	0.68	0.72
160	0.41	0.51	0.41	0.52
165	0.34	0.48	0.33	0.49
170	0.61	0.60	0.59	0.60
175	0.93	0.70	0.94	0.71
180	0.98	0.83	0.98	0.85
185	1.32	1.06	1.37	1.09
190	1.80	1.29	1.94	1.34
195	3.11	1.51	3.25	1.58
200	3.53	1.73	3.88	1.80

The observed excess for m_H from 115 to 140 GeV/c^2 is driven by an excess of data events with respect to the background predictions in the most sensitive bins of the discriminant distributions, favoring the hypothesis that a signal is present. To characterize the compatibility of this excess with the signal-plus-background hypothesis, the best-fit rate parameter, $R^{\rm fit}$, is computed, and shown in Fig. 7. The measured signal strength is within 1 s.d.

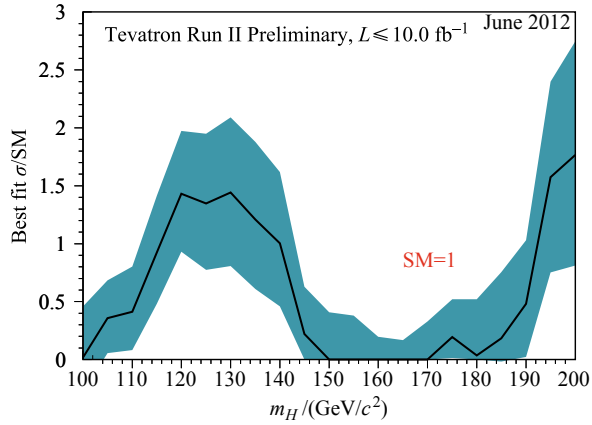

Fig. 7 The best-fit signal cross section of all CDF and D0 search channels combined shown as a ratio to the standard model cross section as a function of the tested Higgs boson mass. The blue band shows the 1 s.d. uncertainty on the signal fit, and the red line is drawn at 1.0, corresponding to the SM prediction. Reproduced from Ref. [1].

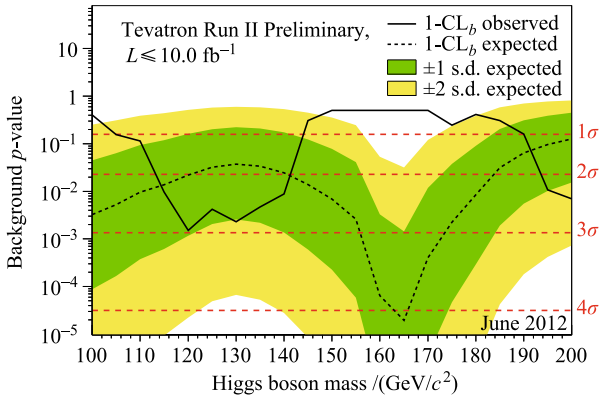

Fig. 8 The solid black line shows the p-value as a function of m_H under the background-only hypothesis, for the combined SM Higgs boson searches. The dotted black line shows the median expected values assuming a SM signal is present, evaluated separately at each m_H. The associated dark and light-shaded bands indicate the one and two s.d. fluctuations of possible experimental outcomes. Reproduced from Ref. [1].

of the expectation for a SM Higgs boson in the range $115 < m_H < 140$ GeV/c^2, with maximal strength around 125 GeV/c^2.

The significance of the excess in the data over the background prediction is computed at each hypothesized Higgs boson mass by calculating the local p-value under the background-only hypothesis using R^{fit} as the test statistic. This p-value expresses the probability to obtain the value of R^{fit} observed in the data or larger, assuming a signal is truly absent. These p-values are shown in Fig. 11 along with the expected p-values assuming a SM signal is present, separately for each value of m_H. The maximum local significance is at $m_H = 120$ GeV/c^2 and corresponds to 3.0 standard deviations. The fluctuations seen in the observed p-value as a function of the tested m_H result from excesses seen in different search channels, as well as from point-to-point fluctuations due to the separate discriminants at each m_H, and are discussed in more detail below. The width of the dip in the p-values from 115 to 140 GeV/c^2 is consistent with the resolution of the combination of the $H \to b\bar{b}$ and $H \to W^+W^-$ channels. The effective resolution of this search comes from two independent sources of information. The reconstructed candidate masses help constrain m_H, but more importantly, the expected cross sections times the relevant branching ratios for the $H \to b\bar{b}$ and $H \to W^+W^-$ channels are strong functions of m_H in the SM. The observed excess in the $H \to b\bar{b}$ channels coupled with the slight excess in the $H \to W^+W^-$ channels determines the shape of the observed p-value as a function of m_H.

The CDF and D0 searches have also been separated into combinations focusing on the $H \to b\bar{b}$, $H \to W^+W^-$ and $H \to \gamma\gamma$ decay channels, and these are discussed in the following sections.

6.3 $H \to b\bar{b}$ decay mode

Below 125 GeV/c^2, the $H \to b\bar{b}$ searches contribute the majority of our sensitivity. The $WH \to \ell\nu b\bar{b}$, $ZH \to \nu\bar{\nu}b\bar{b}$, and $ZH \to \ell^+\ell^- b\bar{b}$ channels from both experiments are included in this sub-combination. The results shown here are taken from Ref. [2]. The observed LLR distribution is shown in Fig. 9, along with its expected values under the background-only and signal-plus-background hypotheses, and also the hypothesis that a SM Higgs boson is present with $m_H = 125$ GeV/c^2.

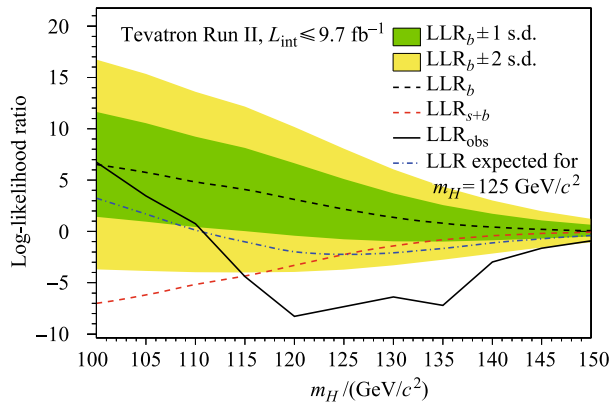

Fig. 9 The log-likelihood ratio LLR as a function of Higgs boson mass for the $H \to b\bar{b}$ analyses. The dark and light-shaded bands correspond to the regions encompassing one and two s.d. fluctuations of the background, respectively. The dot-dashed line shows the median expected LLR assuming the SM Higgs boson is present at $m_H = 125$ GeV/c^2. Reproduced from Ref. [2].

We multiply the best-fit rate parameter for this sub-combination, R^{fit}, by the SM prediction for the associated-production cross section times the decay branching ratio $(\sigma_{WH} + \sigma_{ZH}) \times \mathcal{B}(H \to b\bar{b})$, to obtain the observed value for this quantity. We show our fitted $(\sigma_{WH} + \sigma_{ZH}) \times \mathcal{B}(H \to b\bar{b})$ as a function of m_H, along with the SM prediction, in Fig. 10. The figure also shows the expected cross section fits for each m_H, assuming that the SM Higgs boson with $m_H = 125$ GeV/c^2 is present, both at the rate predicted by the SM, and also at the best-fit rate, which corresponds to $(\sigma_{WH}+\sigma_{ZH}) \times \mathcal{B}(H \to b\bar{b}) = 0.23 \pm 0.09$ (stat + syst) pb. The corresponding SM prediction for $m_H = 125$ GeV/c^2 is 0.12 ± 0.01 pb.

The significance of the excess in the data over the background prediction is computed at each hypothesized Higgs boson mass in the range 100–150 GeV/c^2 by calculating the local p-value under the background-only hypothesis using R^{fit} as the test statistic. These p-values are shown in Fig. 11 along with the expected p-values assuming a SM signal is present, separately for each value of m_H. The maximum local significance corresponds to 3.3

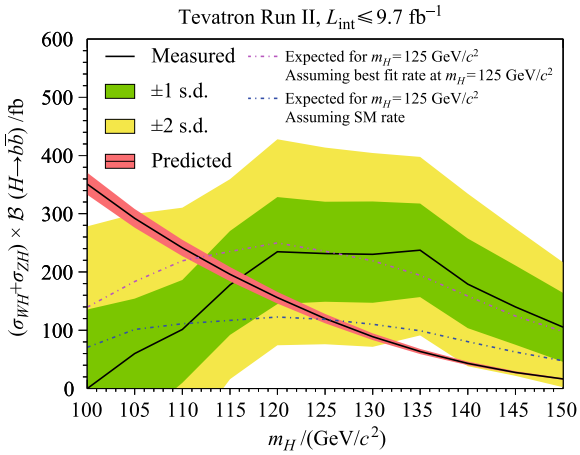

Fig. 10 The best-fit cross section times branching ratio $(\sigma_{WH} + \sigma_{ZH}) \times \mathcal{B}(H \to b\bar{b})$ as a function of m_H. The dark and light-shaded regions indicate the 1 s.d. and 2 s.d. measurement uncertainties, and the SM prediction is shown as the smooth, falling curve with a narrow band indicating the theoretical uncertainty. The expected cross section fit values assuming the SM Higgs boson is present at $m_H = 125$ GeV/c^2 are shown with dot-dashed lines for the cases of the expected SM rate (dark blue) and the best fitted rate from data (light magenta). Reproduced from Ref. [2].

standard deviations at $m_H = 135$ GeV/c^2.

The Look–Elsewhere Effect (LEE) [70, 71] accounts for the possibility of a background fluctuation affecting the local p-value anywhere in the tested m_H range. In the mass range from 115 GeV/c^2 (the prior bound from the LEP2 direct search [14]) to 150 GeV/c^2, the reconstructed mass resolution is typically 15%, and the resulting LEE factor is approximately 2. Correcting for the LEE yields a global significance of 3.1 standard deviations. Taking into account the exclusion limits from the LHC for the SM Higgs boson mentioned earlier, there is no LEE and we derive a significance of 2.8 standard deviations for $m_H = 125$ GeV/c^2.

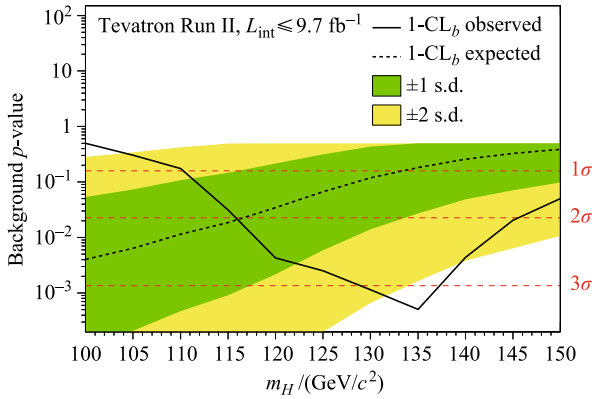

Fig. 11 The p-value as a function of m_H under the background-only hypothesis for the $H \to b\bar{b}$ analyses. Also shown are the median expected values assuming a SM signal is present, evaluated separately at each m_H. The associated dark and light-shaded bands indicate the 1 s.d. and 2 s.d. fluctuations of possible experimental outcomes. Reproduced from Ref. [2].

As discussed in Ref. [2], this result was interpreted as evidence for the presence of a particle that is produced in association with a W or Z boson and decays to a bottom-antibottom quark pair. The excess is most significant in the mass range between 120 and 135 GeV/c^2, and is consistent with production of the SM Higgs boson within this range.

6.4 $H \to W^+W^-$ decay mode

Above 125 GeV/c^2, the $H \to W^+W^-$ channels contribute the majority of our search sensitivity. We combine all $H \to W^+W^-$ searches from CDF and D0, incorporating potential signal contributions from $gg \to H$, WH, ZH, and VBF production. Approximately 75% of the signal comes from the gluon-gluon fusion process, 20% from associated production and 5% from the VBF process. The LLR distribution is shown in Fig. 12. The observed data do not indicate any significant excesses. The data present a one to two s.d. excess in the region from 115 to 140 GeV/c^2 where there is some separation between the two hypotheses.

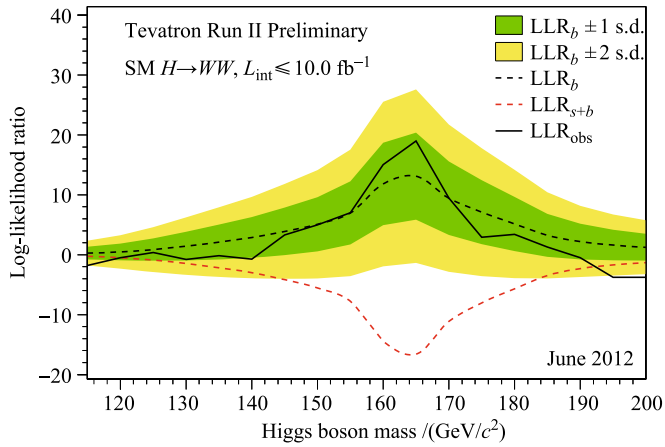

Fig. 12 Distributions of the log-likelihood ratio (LLR) as a function of Higgs boson mass obtained with the CL$_s$ method for the combination of all CDF and D0 analyses for the $H \to W^+W^-$ analyses. The green and yellow bands correspond to the regions enclosing one and two s.d. fluctuations of the background, respectively. Reproduced from Ref. [1].

6.5 $H \to \gamma\gamma$ decay mode

CDF's and D0's searches for $H \to \gamma\gamma$ decays are also combined separately. Figure 13 displays the resulting upper limits on the production cross section times the decay branching ratio normalized to the SM prediction. A slight excess is seen in these searches at $m_H = 125$ GeV/c^2, but the contribution to the SM combined cross section and limit is small due to the small expected signal yield in this channel. This excess in the $H \to \gamma\gamma$ search channel however has a visible impact in the constraints on the

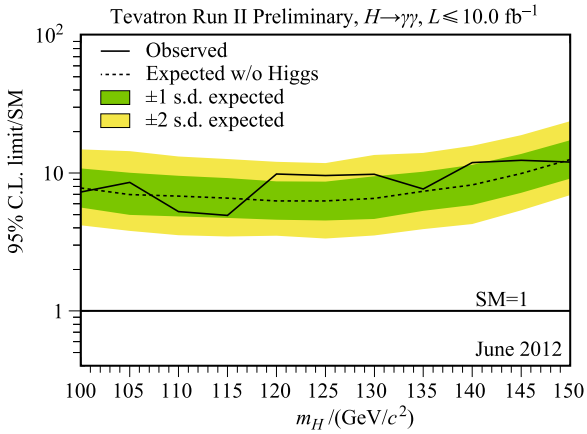

Fig. 13 Observed and expected (median, for the background-only hypothesis) 95% C.L. Bayesian upper limits expressed as a multiple of the SM cross section for test masses every 5 GeV/c^2 for the $H \to \gamma\gamma$ analyses. The points are joined by straight lines for better readability. The bands indicate the 1 and 2 s.d probability regions where the limits can fluctuate, in the absence of signal. Reproduced from Ref. [1].

Higgs boson couplings, as will be seen in Section 6.6.

6.6 Compatibility of the excess with the SM Higgs boson hypothesis

The best-fit rate parameter, R^{fit}, for the full combination of all channels and the $H \to W^+W^-$, $H \to b\bar{b}$ and $H \to \gamma\gamma$ sub-combinations [72] is shown in Table 3 in the range where the combined result has sensitivity to a signal and shows a clear excess, i.e., for 115 GeV/$c^2 \leqslant m_H \leqslant$ 140 GeV/c^2. For $m_H = 125$ GeV/c^2, $R^{\text{fit}} = 1.4 \pm 0.6$ using all decay modes.

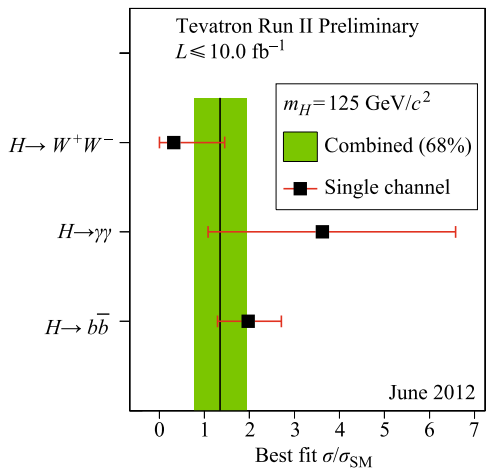

Fig. 14 Best-fit signal strength for the three sub-combinations for $m_H = 125$ GeV/c^2. The shaded band corresponds to the $\pm 1\sigma$ uncertainty on the full combination. Reproduced from Ref. [1].

Figure 14 shows the contribution of the three different sub-combinations to the best-fit signal cross section for $m_H = 125$ GeV/c^2. The results are consistent with each other, the full combination, and with the production of the SM Higgs boson at that mass.

Table 3 Measurements of the best-fit values of $R = \sigma \times \mathcal{B}/\text{SM}$ using the Bayesian method, for the combined SM, $H \to W^+W^-$, $H \to b\bar{b}$ and $H \to \gamma\gamma$ searches, for 115 GeV/$c^2 \leqslant m_H \leqslant$ 140 GeV/c^2. The quoted uncertainties bound the smallest interval containing 68% of the integral of the posterior probability densities.

m_H/(GeV/c^2)	R_{fit} (SM)	R_{fit} ($H \to WW$)	R_{fit} ($H \to b\bar{b}$)	R_{fit} ($H \to \gamma\gamma$)
115	$0.92^{+0.49}_{-0.44}$	$3.50^{+2.08}_{-2.13}$	$0.90^{+0.47}_{-0.45}$	$0.00^{+2.47}_{-0.00}$
120	$1.43^{+0.54}_{-0.50}$	$0.90^{+1.24}_{-0.90}$	$1.52^{+0.57}_{-0.58}$	$4.17^{+2.95}_{-2.54}$
125	$1.35^{+0.60}_{-0.57}$	$0.32^{+1.13}_{-0.32}$	$1.97^{+0.74}_{-0.68}$	$3.62^{+2.96}_{-2.54}$
130	$1.44^{+0.65}_{-0.64}$	$0.81^{+0.70}_{-0.71}$	$2.39^{+0.93}_{-0.94}$	$3.72^{+2.91}_{-2.78}$
135	$1.21^{+0.67}_{-0.60}$	$0.44^{+0.60}_{-0.44}$	$3.53^{+1.26}_{-1.16}$	$0.00^{+4.13}_{-0.00}$
140	$1.00^{+0.62}_{-0.54}$	$0.69^{+0.54}_{-0.52}$	$4.24^{+1.74}_{-1.70}$	$3.85^{+3.52}_{-3.31}$

7 Interpretations beyond-the-SM

The mechanism of electroweak symmetry breaking may offer a richer phenomenology than expected in the SM. Many beyond-the-standard model Higgs boson searches have been carried out at Tevatron, including results in models with a sequential fourth generation of fermions, the fermiophobic Higgs model and the minimimal supersymmetric standard model (MSSM); for full details see http://www-cdf.fnal.gov/physics/physics.html and http://www-d0.fnal.gov/Run2Physics/WWW/results.htm. Here the latest results in the search for neutral Higgs bosons produced in the multi-b-jet topology is discussed.

7.1 Search for neutral higgs bosons in the multi-b-jet topology

Introducing a second Higgs doublet, such as in type II 2-Higgs doublet models (2HDM) [73], leads to multiple scalar bosons and can give scenarios with enhanced couplings to down-type fermions. Supersymmetry is a plausible extension to the SM that introduces an additional symmetry between fermions and bosons. The two Higgs boson doublets in the minimal supersymmetric standard model (MSSM) [74, 75] lead to five physical Higgs bosons: three neutral (collectively denoted as ϕ): h, H, and A; and two charged: H^+ and H^-. At leading order the MSSM is a type II 2HDM model, and two parameters are sufficient to describe the Higgs sector, conventionally chosen as the ratio of the two Higgs doublet vacuum expectation values, $\tan\beta$, and, M_A, the mass of the pseudoscalar boson, A. The couplings to the down-type fermions are enhanced by a factor of $\tan\beta$ relative to those in the SM. Thus, the main decay mode is $\phi \to b\bar{b}$, with branching fractions near 90% at leading

order (the remainder being mostly $\phi \to \tau^+\tau^-$). Since an inclusive search for $\phi \to b\bar{b}$ is difficult due to large multijet backgrounds, these searches rely on the case where the ϕ boson is produced in association with one or more b quarks. This final state with at least three b quarks represents a powerful search channel, with the third b jet providing additional suppression of the large multijet background at a hadron collider.

MSSM Higgs boson production has been studied at the CERN LEP e^+e^- collider excluding $M_{h,A} < 93$ GeV for all $\tan\beta$ values [76]. The CDF [77–79] and D0 [80–89] collaborations extended such searches to higher masses and for large $\tan\beta$. The most stringent upper limits on $\tan\beta$ in searches for neutral Higgs production for masses above the LEP bounds come from searches in final states with τ leptons pair produced at the Large Hadron Collider [90–92]. The results discussed here are taken from Ref. [3], and are based on the combination of results from the CDF and D0 Collaborations, using integrated luminosities of 2.6 fb^{-1} and 5.2 fb^{-1}respectively [79, 86].

At CDF, the background is modeled using a sum of templates of the invariant mass distribution of the two jets with the highest p_T, representing contributions from different background modes categorized according to kinematics and flavor content. The templates are constructed from events in the double-tagged data sample where at least one of the two highest-p_T jets is b-tagged. The events are then weighted according to the probability for at least one of the jets with no b tag to pass the tagging requirements under three different assumptions as to whether it arises from a b quark, a c quark or a light quark (or gluon). This results in six different mass templates. The separation between the different components is enhanced by using an additional jet-flavor-sensitive discriminant, $x_{\rm tags}$, that makes use of kinematic properties of the charged particles from secondary vertices associated with each b-tagged jet.

In the D0 analysis the background model is formed by correcting the shape of the dijet invariant mass distribution of a data sample with two b-tagged jets using the ratio of simulated multijet samples with three b tags and two b tags. The simulated samples are generated using ALPGEN with showering and hadronization carried out using PYTHIA and detailed simulation of the detector using GEANT. Their flavor composition, in terms of the relative numbers of b, c and light jets per event, is determined from a simultaneous fit to the data across samples with differing numbers of tagged jets, different b-tagger operating points, and in small intervals of the scalar sum of the transverse momenta of the jets. The shape correction is applied as a function of the dijet invariant mass and the value of a likelihood-ratio discriminant, $\mathcal{L}$, designed to select signal-like events in preference to background-like events. Only the two jet pairings from the highest p_T jet plus either the second or third highest p_T jet, are considered when forming Higgs candidates, and the choice that gives the highest value of $\mathcal{L} > 0.65$ is selected. If neither pairing in the event is above this threshold then the event is discarded. Systematic uncertainties are assessed to take into account the imperfect modeling of the background simulation. However, the definition of the correction as a ratio of distributions significantly reduces the sensitivity of the final model to these imperfections. Small contributions to the background from top-quark-pair production are simulated using ALPGEN and PYTHIA. Backgrounds from other sources, such as $Z \to b\bar{b}$ and single-top-quark production are negligible.

Associated production of a ϕ boson and a b quark, $gb \to \phi b$, with subsequent decay $\phi \to b\bar{b}$, as modelled by PYTHIA is used to model the signal. The signal cross section, experimental acceptance and the kinematics are corrected to next-to-leading order using MCFM, weighting events as a function of the kinematics of the highest p_T b-quark jet not associated with the Higgs decay.

The channels are combined and exclusion limits set, using the modified frequentist technique with a log-likelihood test statistic as in the SM case. The likelihoods are constructed from the binned two-dimensional distribution of the dijet invariant mass versus the $x_{\rm tags}$ discriminant for CDF and the binned one-dimensional dijet invariant mass distribution for D0. Theoretical predictions of the absolute rates for the multijet backgrounds have large uncertainties. Therefore, additional scale factors are applied to the background yield in the D0 analysis and the individual templates in the CDF analysis and introduced into the likelihood as parameters with no external constraints. Systematic uncertainties are introduced as either shape or normalization variations to the model probability density functions.

Quasi-model-independent limits on the product of the cross section and the branching ratio using the LLR test statistic are extracted and presented in Fig. 15. Excesses of events above the SM background expectation are observed for $M_\phi = 120$ and 140 GeV with significances of 2.5 s.d. and 2.6 s.d., respectively. These are driven by the excesses observed in the individual contributing analyses of 2.8 s.d. at $M_\phi = 150$ GeV at CDF and 2.5 s.d. at $M_\phi = 120$ GeV at D0. Including an appropriate trials factor reduces the significance of the excesses in the combined analysis to ≈ 2 s.d.

Though these limits are the key results of this search, it is interesting to interpret them in terms of constraints on benchmark models within the MSSM. When interpreting the exclusion within the MSSM, the width of the Higgs boson and the enhancement of the product of cross

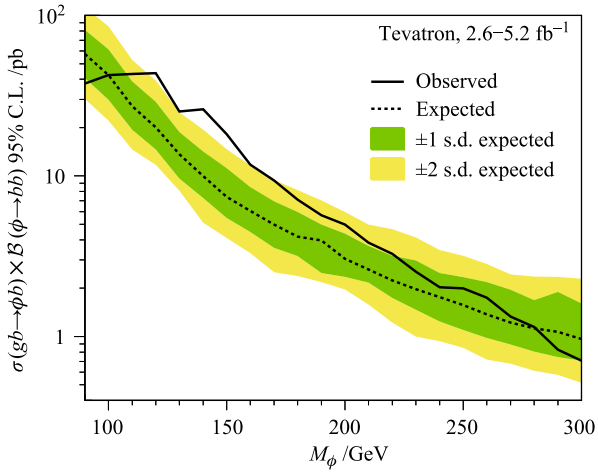

Fig. 15 Model-independent 95% C.L. upper limits on the product of cross section and branching ratio for the combined analyses, assuming a Higgs boson width significantly smaller than the experimental resolution. The dark and light shaded regions correspond to the 1 and 2 s.d. bands around the median expected limit. Reproduced from Ref. [3].

section and branching ratio above that of the SM are calculated using FEYNHIGGS [93–98]. The width is included in the simulation of the signal as a function of mass and $\tan\beta$ by convoluting a relativistic Breit–Wigner function with the next-to-leading cross section. Additional uncertainties for these model-specific limits are considered that otherwise cancel in the model-independent limit.

Limits on $\tan\beta$ as a function of M_A are derived for the $m_h^{\max}$ scenario [99] that favors the $b\bar{b}$ final state, assuming a CP-conserving Higgs sector [100] and a negative value of the Higgs sector bilinear coupling μ. Figure 16 shows exclusion limits in the $(\tan\beta, M_A)$ plane for this scenario. Adding a further potential theoretical uncertainty on the signal cross section of 20%, independent of M_ϕ, would lead to an increase of 5% in the $\tan\beta$ limit.

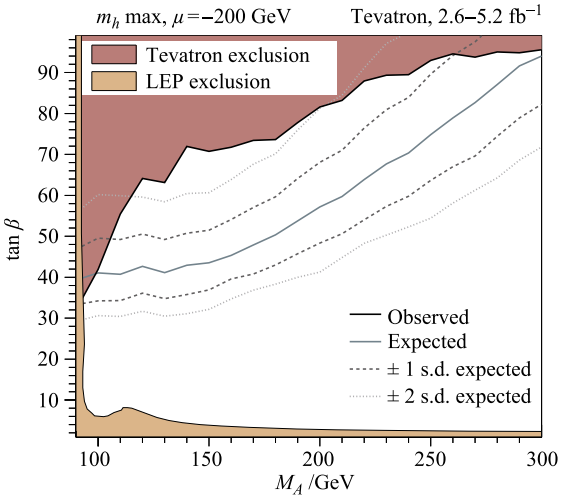

Fig. 16 95% C.L. lower limit in the (M_A, tanβ) plane for the $m_h^{\max}, \mu = -200$ GeV, including Higgs boson width effects and using the fact that for the tan βrange considered, either h and A, or H and A (depending on M_A) are effectively mass degenerate. The exclusion limit obtained from the LEP experiments is also shown. Reproduced from Ref. [3].

8 Conclusions

The search for the standard model Higgs boson at the Tevatron is challenging due to the small expected signal and the large backgrounds with associated systematic uncertainties. We have developed tools to search for the Higgs boson in the leading production and decay modes predicted by the SM, and control the impacts of systematic uncertainties using constraints from the measured data. The combined searches by the CDF and D0 Collaborations for the standard model Higgs boson in the the mass range 100–200 GeV/c^2 using $p\bar{p}$ collision data corresponding to up to 10 fb^{-1} collected at $\sqrt{s} = 1.96$ TeV at the Tevatron, are discussed [1, 2]. The results of searches for the $H \to b\bar{b}$, $H \to W^+W^-$ and $H \to \gamma\gamma$ decay modes are included in the combination. The SM Higgs boson is excluded, at the 95% C.L., from 100 to 103 GeV/c^2, and from 147 to 180 GeV/c^2; the expected exclusion regions are 100 – 120 GeV/c^2 and 139 – 184 GeV/c^2. We observe a significant excess of events in the mass range between 115 and 140 GeV/c^2, with a local significance of ≈ 3 Gaussian standard deviations. The best-fit signal strength at $m_H = 125$ GeV/c^2 is 1.4 ± 0.6. We also separately combine searches for $H \to b\bar{b}$, $H \to W^+W^-$, and $H \to \gamma\gamma$. The observed best-fit signal strengths in all channels are consistent with the expectation for a SM Higgs boson at $m_H = 125$ GeV/c^2. The production of neutral Higgs bosons in association with b-quarks can be significantly enhanced in various beyond the standard model scenarios, including Supersymmetry. The recent combination of such searches from the two collaborations is discussed [3].

Acknowledgements We thank the Fermilab staff and technical staffs of the participating institutions for their vital contributions and acknowledge support from the DOE and NSF (USA), ARC (Australia), CNPq, FAPERJ, FAPESP and FUNDUNESP (Brazil), NSERC (Canada), NSC, CAS and CNSF (China), Colciencias (Colombia), MSMT and GACR (Czech Republic), the Academy of Finland, CEA and CNRS/IN2P3 (France), BMBF and DFG (Germany), DAE and DST (India), SFI (Ireland), INFN (Italy), MEXT (Japan), the Korean World Class University Program and NRF (Korea), CONACyT (Mexico), FOM (Netherlands), MON, NRC KI and RFBR (Russia), the Slovak R&D Agency, the Ministerio de Ciencia e Innovación, and Programa Consolider-Ingenio 2010 (Spain), The Swedish Research Council (Sweden), SNSF (Switzerland), STFC and the Royal Society (United Kingdom), and the A.P. Sloan Foundation (USA).

References and notes

1. T. Aaltonen, et al. [CDF and D0 Collaborations], arXiv:

1207.0449, 2012

2. T. Aaltonen, et al. [CDF and D0 Collaborations], Phys. Rev. Lett., 2012, 109: 071804
3. T. Aaltonen, et al. [CDF and D0 Collaborations], Phys. Rev. D, 2012, 85: 032005
4. S. L. Glashow, Nucl. Phys., 1961, 22(4): 579
5. S. Weinberg, Phys. Rev. Lett., 1967, 19(21): 1264
6. A. Salam, Elementary Particle Theory, edited by N. Svartholm, Stockholm: Almqvist & Wiksell, 1968: 367
7. F. Englert and R. Brout, Phys. Rev. Lett., 1964, 13(9): 321
8. P. W. Higgs, Phys. Rev. Lett., 1964, 13(16): 508
9. G. S. Guralnik, C. R. Hagen, and T. W. B. Kibble, Phys. Rev. Lett., 1964, 13(20): 585
10. P. W. Higgs, Phys. Rev., 1966, 145(4): 1156
11. T. Aaltonen, et al. [CDF and D0 Collaborations], arXiv: 1204.0042, 2012
12. T. Aaltonen, et al. [CDF and D0 Collaborations], Phys. Rev. D, 2012, 86: 092003
13. The ALEPH, CDF, D0, DELPHI, L3, OPAL, and SLD Collaborations, the LEP Electroweak Working Group, the Tevatron Electroweak Working Group, and the SLD Electroweak and Heavy Flavor Working Groups, arXiv: 1012.2367v2, 2011
14. The ALEPH, DELPHI, L3 and OPAL Collaborations, and the LEP Working Group for Higgs Boson Searches, Phys. Lett. B, 2003, 565: 61
15. G. Aad, et al. [ATLAS Collaboration], Phys. Lett. B, 2012, 716: 1
16. S. Chatrchyan, et al. [CMS Collaboration], Phys. Lett. B, 2012, 716: 30
17. G. Aad, et al. [ATLAS Collaboration], arXiv: 1207.0210, 2012; submitted to Phys. Lett. B.
18. S. Chatrchyan, et al. [CMS Collaboration], Phys. Lett. B, 2012, 710: 284
19. CDF and D0 use cylindrical coordinate systems with origins in the centers of the detectors, where θ and φ are the polar and azimuthal angles, respectively, and pseudora pidity is $\eta = -\ln\tan(\theta/2)$. The missing E_T ($\vec{\not\!\!E}_T$) is defined by $\vec{\not\!\!E}_T = -\sum_i E_T^i \hat{n}_i$, i = calorimeter tower number, where $\hat{n}_i$ is a unit vector perpendicular to the beam axis and pointing at the ith calorimeter tower. $\vec{\not\!\!E}_T$ is corrected for high-energy muons and also jet energy corrections. We define $\not\!\!E_T = |\vec{\not\!\!E}_T|$. The transverse momentum p_T is defined to be $p \sin\theta$.
20. T. Sjöstrand, S. Mrenna, and P. Skands, J. High Energy Phys., 2006, 05: 026. We use pythia version 6.216 to generate the Higgs boson signals.
21. H. L. Lai, J. Huston, S. Kuhlmann, J. Morfin, F. Olness, J. F. Owens, J. Pumplin, and W. K. Tung, Eur. Phys. J. C, 2000, 12(3): 375
22. J. Pumplin, et al., J. High Energy Phys., 2002, 07: 012
23. C. Anastasiou, R. Boughezal, and F. Petriello, J. High Energy Phys., 2009, 04: 003
24. D. de Florian and M. Grazzini, Phys. Lett. B, 2009, 674(4-5): 291
25. J. Baglio and A. Djouadi, J. High Energy Phys., 2010, 10: 064
26. O. Brein, R. V. Harlander, M. Weisemann, and T. Zirke, Eur. Phys. J. C, 2012, 72(2): 1868
27. P. Bolzoni, F. Maltoni, S. O. Moch, and M. Zaro, Phys. Rev. Lett., 2010, 105(1): 011801
28. M. Ciccolini, A. Denner, and S. Dittmaier, Phys. Rev. Lett., 2007, 99(16): 161803
29. M. Ciccolini, A. Denner, and S. Dittmaier, Phys. Rev. D, 2008, 77(1): 013002
30. A. D. Martin, W. J. Stirling, R. S. Thorne, and G. Watt, Eur. Phys. J. C, 2009, 63(2): 189
31. S. Alekhin, et al. [PDF4LHC Working Group], arXiv: 1101.0536, 2011
32. M. Botje, et al. [PDF4LHC Working Group], arXiv: 1101.0538, 2011
33. C. Anastasiou, G. Dissertori, M. Grazzini, F. Stöckli, and B. R. Webber, J. High Energy Phys., 2009, 08: 099
34. S. Dittmaier, et al. [LHC Higgs Cross Section Working Group], arXiv: 1201.3084, 2012
35. A. Djouadi, J. Kalinowski, and M. Spira, Comput. Phys. Commun., 1998, 108(1): 56
36. A. Bredenstein, A. Denner, S. Dittmaier, and M. M. Weber, Phys. Rev. D, 2006, 74(1): 013004
37. A. Bredenstein, A. Denner, S. Dittmaier, A. Mück, and M. M. Weber, J. High Energy Phys., 2007, 02: 080
38. G. Bozzi, S. Catani, D. de Florian, and M. Grazzini, Phys. Lett. B, 2003, 564(1–2): 65
39. G. Bozzi, S. Catani, D. de Florian, and M. Grazzini, Nucl. Phys. B, 2006, 737(1–2): 73
40. M. Mangano, M. Moretti, F. Piccinini, R. Pittau, and A. Polosa, J. High Energy Phys., 2003, 07: 001
41. S. Frixione and B. R. Webber, J. High Energy Phys., 2002, 06: 029
42. G. Corcella, I. G. Knowles, G. Marchesini, S. Moretti, K. Odagiri, P. Richardson, M. H. Seymour, and B. R. Webber, J. High Energy Phys., 2001, 01: 010
43. A. Pukhov, E. Boos, M. Dubinin, V. Edneral, V. Ilyin, D. Kovalenko, A. Kryukov, V. Savrin, S. Shichanin, and A. Semenov, arXiv: hep-ph/9908288, 1999
44. E. Boos, V. Bunichev, M. Dubinin, L. Dudko, V. Ilyin, A. Kryukov, V. Edneral, V. Savrin, A. Semenov, and A. Sherstnev, Nucl. Instrum. Methods Phys. Res.: Sect. A, 2004, 534: 250
45. E. E. Boos, V. E. Bunichev, L. V. Dudko, V. I. Savrin, and A. V. Sherstnev, Phys. At. Nucl., 2006, 69(8): 1317
46. J. M. Campbell and R. K. Ellis, Phys. Rev. D, 1999, 60(11): 113006
47. U. Langenfeld, S. Moch, and P. Uwer, Phys. Rev. D, 2009, 80(5): 054009
48. N. Kidonakis, Phys. Rev. D, 2006, 74(11): 114012

49. R. Hamberg, W. L. van Neerven, and T. Matsuura, Nucl. Phys. B, 1991, 359(2–3): 343; Erratum, Nucl. Phys. B, 2002, 644: 403
50. A heavy-flavor jet is a reconstructed cluster of calorimeter energies associated with particles produced in the hadronization and decay of a bottom or charm quark.
51. A B-tagged jet is one identified to have originated from the decay of a heavy flavor quark.
52. D. Acosta, et al. [CDF Collaboration], Phys. Rev. D, 2005, 71: 032001
53. A. Abulencia, et al. [CDF Collaboration], J. Phys. G, 2007, 34: 2457
54. V. M. Abazov, et al. [D0 Collaboration], Nucl. Instrum. Methods Phys. Res.: Sect. A, 2006, 565: 463
55. M. Abolins, et al., Nucl. Instrum. Methods Phys. Res.: Sect. A, 2008, 584: 75
56. R. Angstadt, et al., Nucl. Instrum. Methods Phys. Res.: Sect. A, 2010, 622: 298
57. For a recent review, see: P. C. Bhat, Ann. Rev. Nucl. Part. Sci., 2011, 61(1): 281. The specific details of each analysis's MVA are described in the respective references.
58. V. M. Abazov, et al., Nucl. Instrum. Methods Phys. Res.: Sect. A, 2010, 620: 490
59. J. Freeman, et al., Nucl. Instrum. Methods Phys. Res.: Sect. A, 2013, 697: 64
60. D. Acosta, et al. [CDF Collaboration], Phys. Rev. D, 2005, 71: 052003
61. A. Abulencia, et al. [CDF Collaboration], Phys. Rev. D, 2006, 74: 072006
62. Statistics, in: K. Nakamura, et al. [Particle Data Group], J. Phys. G, 2010, 37: 075021.
63. T. Aaltonen, et al. [CDF Collaboration], Phys. Rev. Lett., 2012, 109(11): 111802
64. V. M. Abazov, et al. [D0 Collaboration], Phys. Rev. Lett., 2012, 109(12): 121802
65. W. Fisher, FERMILAB-TM-2386-E, 2006
66. T. Junk Nucl. Instrum. Methods Phys. Res.: Sect. A, 1999, 434: 435
67. A. L. Read, J. Phys. G, 2002, 28(10): 2693
68. I. W. Stewart and F. J. Tackmann, Phys. Rev. D, 2012, 85(3): 034011
69. J. M. Campbell, R. K. Ellis, and C. Williams, Phys. Rev. D, 2010, 81(7): 074023
70. L. Lyons, Annals of Applied Statistics, 2008, 2(3): 887
71. O. J. Dunn, J. Am. Stat. Assoc., 1961, 56(293): 52
72. A particular decay mode defined by an experimental signature as done here may be an admixture of several, though dominated by the one denoted.
73. V. Barger, J. L. Hewett, and R. J. N. Phillips, Phys. Rev. D, 1990, 41(11): 3421
74. H. P. Nilles, Phys. Rep., 1984, 110(1–2): 1
75. H. E. Haber, and G. L. Kane, Phys. Rep., 1985, 117(2–4): 75
76. The ALEPH Collaboration, The DELPHI Collaboration, The L3 Collaboration, and The OPAL Collaboration, Eur. Phys. J. C, 2006, 47: 547
77. T. Affolder, et al. [CDF Collaboration], Phys. Rev. Lett., 2001, 86: 4472
78. A. Abulencia, et al. [CDF Collaboration], Phys. Rev. Lett., 2006, 96: 011802
79. T. Aaltonen, et al. [CDF Collaboration], Phys. Rev. D, 2012, 85: 032005
80. V. M. Abazov, et al. [D0 Collaboration], Phys. Rev. Lett., 2005, 95(15): 151801
81. V. M. Abazov, et al. [D0 Collaboration], Phys. Rev. Lett., 2006, 97(12): 121802
82. V. M. Abazov, et al. [D0 Collaboration], Phys. Rev. Lett., 2008, 101(7): 071804
83. V. M. Abazov, et al. [D0 Collaboration], Phys. Rev. Lett., 2008, 101(22): 221802
84. V. M. Abazov, et al. [D0 Collaboration], Phys. Rev. Lett., 2009, 102(5): 051804
85. V. M. Abazov, et al. [D0 Collaboration], Phys. Rev. Lett., 2010, 104(15): 151801
86. V. M. Abazov, et al. [D0 Collaboration], Phys. Lett. B, 2011, 698: 97
87. V. M. Abazov, et al. [D0 Collaboration], Phys. Rev. Lett., 2011, 107(12): 121801
88. V. M. Abazov, et al. [D0 Collaboration], Phys. Lett. B, 2012, 707: 323
89. V. M. Abazov, et al. [D0 Collaboration], Phys. Lett. B, 2012, 710: 569
90. CMS Collaboration, Phys. Rev. Lett., 2011, 106: 231801
91. ATLAS Collaboration, Phys. Lett. B, 2011, 705: 174
92. CMS Collaboration, Phys. Lett. B, 2012, 713: 68
93. S. Heinemeyer, W. Hollik, and G. Weiglein, Eur. Phys. J. C, 1999, 9: 343, FEYNHIGGS version 2.6.8 is used.
94. S. Heinemeyer, W. Hollik, and G. Weiglein, Comput. Phys. Commun., 2000, 124(1): 76
95. G. Degrassi, S. Heinemeyer, W. Hollik, P. Slavich, and G. Weiglein, Eur. Phys. J. C, 2003, 28(1): 133
96. M. Frank, T. Hahn, S. Heinemeyer, W. Hollik, H. Rzehak, and G. Weiglein, J. High Energy Phys., 2007, 02: 047
97. L. Hofer, U. Nierste, and D. Shere, J. High Energy Phys., 2009, 10: 081
98. D. Noth and M. Spira, Phys. Rev. Lett., 2008, 101(18): 181801
99. $M_{\rm SUSY} = 1$ TeV, $X_t = 2$ TeV, $M_2 = 0.2$ TeV, $|\mu| = 0.2$ TeV, and $m_g = 0.8$ TeV.
100. M. Carena, S. Heinemeyer, C. E. M. Wagner, and G. Weiglein, Eur. Phys. J. C, 2006, 45(3): 797